Microstructural evolution and mechanical properties of thermomechanically processed AZ31 magnesium alloy reinforced by micro-graphite and nano-graphene particles

F. Vahedi, A. Zarei-Hanzaki, A. Salandari-Rabori, H.R. Abedi, A. Razaghian, P. Minarik

PII: S0925-8388(19)33477-2

DOI: https://doi.org/10.1016/j.jallcom.2019.152231

Reference: JALCOM 152231

To appear in: *Journal of Alloys and Compounds*

Received Date: 16 April 2019

Revised Date: 10 August 2019

Accepted Date: 9 September 2019

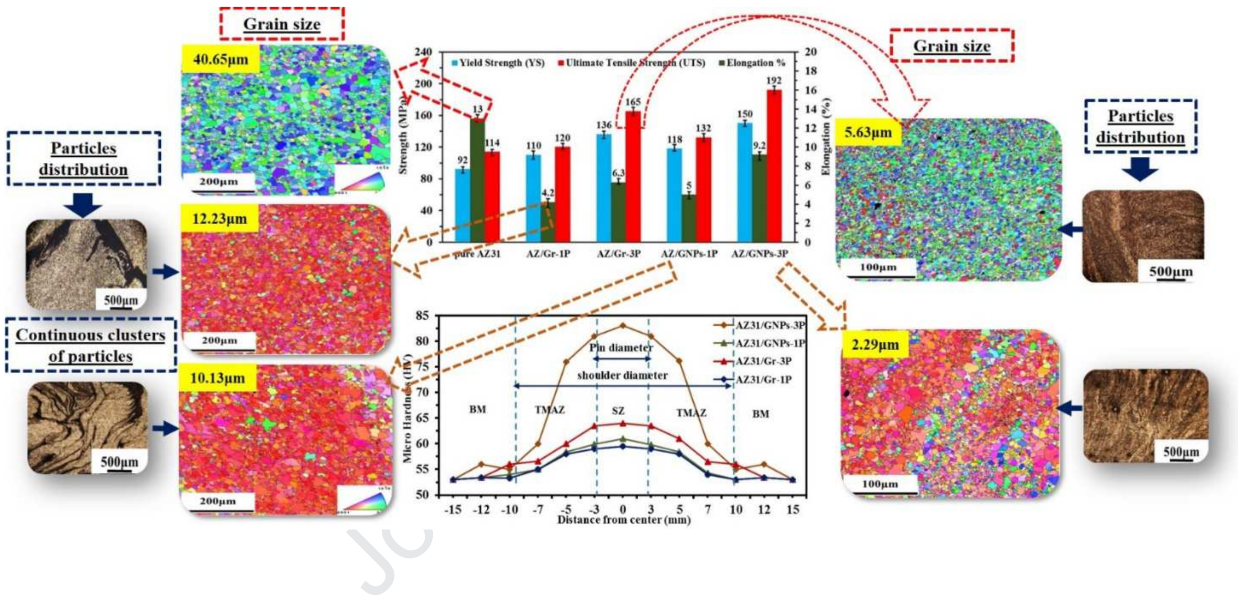
Grain size
40.65μm
200μm
Particles distribution
500μm
12.23μm
200μm
Continuous clusters of particles
500μm
10.13μm
200μm
Yield Strength (YS)
Ultimate Tensile Strength (UTS)
Elongation %
Strength (MPa)
Elongation (%)
92
13
114
110
4.2
120
136
6.3
165
118
5
132
150
9.2
192
pure AZ31
AZ/Gr-1P
AZ/Gr-3P
AZ/GNPs-1P
AZ/GNPs-3P
AZ31/GNPs-3P
AZ31/GNPs-1P
AZ31/Gr-3P
AZ31/Gr-1P
Pin diameter
shoulder diameter
BM
TMAZ
SZ
TMAZ
BM
Micro Hardness (HV)
Distance from center (mm)
Grain size
5.63μm
100μm
Particles distribution
500μm
2.29μm
100μm
500μm

Microstructural evolution and mechanical properties of thermomechanically processed AZ31 magnesium alloy reinforced by micro-graphite and nano-graphene particles

F. Vahedi[a, b], A. Zarei-Hanzaki[b, 1], A. Salandari-Rabori[b, c], H. R. Abedi[b,2], A. Razaghian[a], P. Minarik[d]

[a] Imam Khomeini International University, Qazvin, Iran.

[b] The Complex Laboratory of Hot Deformation and Thermomechanical Processing of High-Performance Engineering Materials, Department of Metallurgy and Materials Engineering, College of Engineering, University of Tehran, Tehran, Iran.

[c] Department of Mechanical and Materials Engineering, Faculty of Engineering and Applied Science, Queen's University, Kingston, Ontario, Canada.

[d] Department of Physics of Materials, Charles University, Prague, Czech Republic.

Abstract

In the present work, microstructural evolution and mechanical properties of a frictionally stir processed magnesium alloy reinforced with micro and nanoparticles were comprehensively investigated. Microstructural characterizations after the first deformation pass for both composites just implied a limited grain refinement along with the agglomeration/clustering of particles, and the difference between two composites was ignorable. While, deformation up to three FSP passes astonishingly followed a different trend, relative to the first pass. Achievement of a fine and homogenous microstructure in conjunction with the evolution of well-distributed particles and almost no sign of clusters were the outcomes of the third pass. Particularly, for the nanocomposite, a fine grain size of 2.29 μm is achieved. Additionally, better mechanical properties including higher values of Vickers microhardness and yield and also ultimate tensile strengths were attained after the third pass, compared to the first one. Better distribution of nanoparticles and their decisive role in improving tensile properties, compared to microparticles, led to the achievement of high hardness of 83 HV and ultimate tensile strength of 192 MPa for the graphene nanocomposite. Furthermore, the change from a brittle fracture to the brittle-ductile and ductile fracture is observed for micro and nanoparticles after the third FSP pass.

Keywords: Magnesium alloys; Nano-composite; Graphene; Graphite; Thermomechanical processing

---

[1] Corresponding author.
Email Address: zareih@ut.ac.ir (Abbas Zarei-Hanzaki)
[2] Co-corresponding author.
Email Address: Habedi@ut.ac.ir (Hamid Reza Abedi)

1. Introduction

The carbonaceous family is considered as the most attractive reinforcing materials compared to other ceramic reinforcements due to their high thermal conductivity, low thermal expansion coefficient, good self-lubricant properties and high damping capacity [1,2]. Additionally, the low density of this group of materials makes them the best choice for applications in aerospace industries and composite materials. Graphite (Gr) and graphene are the oldest and newest members of this family, respectively [3]. Earlier researchers have reported that during the dry sliding of the metal/Gr composites a continuous layer of solid lubricant is formed on the tribological surface. This phenomenon occurs due to the shearing of Gr particles which are located underneath the sliding surface and thereby helps in reducing the shear stress [4,5]. Wear properties of copper-graphite composites fabricated by friction stir processing (FSP) was studied by Sarmadi et al. [6]. They described that an increase in the graphite content led to the significant decrease in the friction coefficient, as well as the decrease in the number of metal to metal contact points, due to the presence of graphite particles as a solid lubricant. Furthermore, the hardness of the processed zone considerably increased (about 2 times of pure Cu).

Graphene is the graphite single layer and new two-dimensional carbonaceous material showing unique mechanical and thermal properties because of its superior tensile strength along with the young modulus, which gives rise to great potential as a strengthening element in composites, especially metal matrix composites (MMCs) for structural and functional applications [7]. Chen et al. [8] have produced magnesium matrix composites reinforced by graphene nanoparticles (GNPs) by using liquid state ultrasonic processing and solid-state stirring. They found that GNPs are uniformly dispersed through the matrix and significantly enhanced the microhardness of Mg substrate, about %78 higher than that of the matrix. It also was shown that the GNPs plays a prominent role in strengthening the magnesium matrix composites produced by various techniques [9–11]. These findings confirm the appropriateness of the graphene as reinforcing particles in composites.

The main challenges for the development of MMCs using this group of materials for industrial applications are the attainment of the homogeneous dispersion of carbonaceous reinforcing materials in the metal substrate, the formation of strong interfacial bonding and the retention of structural stability of carbonaceous materials [12]. As recognized, carbon nanomaterials of large surface areas tend to agglomerate into clusters to reduce their surface energy during the composite processing. Many processing was used for the fabrication of these composites such as plasma spraying [13], high-energy laser melt treatment [14], etc. Still, these processings are based on a liquid phase at high temperatures; therefore, not only is the surface reaction prevention between reinforcement particles impossible but also the production of useless phases is unavoidable. Furthermore, the critical control of processing parameters is necessary to obtain ideal solidified microstructures in composites. Obviously, if the processing of surface composites is carried out at temperatures below the melting point of the substrate, the abovementioned problems can be effectively avoided [15]. As well, recently other surface modification methods based on the coating deposition have been used extensively for surface engineering of Mg alloys [16–18].

Friction stir processing based on friction stir welding is a novel solid-state technique which was developed by Mishra et al. [19,20], in this case, the rotating tool is inserted in a substrate for localized microstructural modification for specific properties enhancement. This act produces a plastically high deformed zone during processing which thereby causes the formation of fine and equiaxed grains in the stir zone due to the refined grains by recrystallization and the homogenization of reinforcement particles. These characteristics made FSP a promising way to produce improved composites. Over recent years, several studies regarding the surface layer modification of metallic alloys have been reported. Mishra et al. [21] fabricated Al/SiC surface composite by FSP and the noticeable increase in the tensile strength and the hardness of the stir zone by improving the distribution of reinforcing particles through regulating FSP parameters was reported. Similar results were also obtained in the production of various Mg and Al-based surface composites by FSP which emphasized the undeniable role of FSP processing in improving the composites' properties [22–25].

Nonetheless, most of the accomplished studies dealing with GNPs and graphite reinforced composites are based on Al and other metallic alloys substrate, and they chiefly have focused on wear properties. Thus, there are limited works regarding Mg/GNPs and Mg/Gr composites fabricated by severe plastic deformation (SPD) techniques, especially FSP. In the present study, FSP was used to fabricate magnesium matrix composite reinforced by two kinds of carbonaceous materials, graphite micro size particles, and graphene nanoplatelets. The effect of each particle on microstructural evolution, grain refinement mechanisms, recrystallization mechanisms, mechanical properties (hardness and tensile properties) and fracture surfaces (fractography) after one and three FSP trials have been thoroughly evaluated.

2. Experimental procedure

The experimental AZ31 magnesium alloy was received in the form of a hot-rolled ingot. The chemical composition of the experimental alloy is presented in Table 1. The initial microstructure is depicted in forms of inverse pole figure (IPF) maps in Fig. 1a, where the majority of grains are equiaxed and the average grain size (Fig. 1b) is 40.65 μm. Fig. 1c indicates the schematic of FSP and processing directions, and also the location of sampling for microstructural characterizations. Available commercial micro-size Gr particles by an average diameter of 25 μm and density of 2.2 g/cm^3 along with grade C of GNPs by a thickness of 1-20 nm, a width of 10-50 μm, and density of 1.06 g/cm^3 were used as reinforcing particles. The volume fraction of both particles is approximately %7.4, which was calculated from employed methods in the literature [26]. Fig. 2 shows the micro and nanoparticles used in the current work. For FSP processing, the initial experimental alloy was sliced to samples with 10 mm thickness, 150 mm length and 100 mm width using the wire electro-discharge machine (EDM).

A groove by 1 mm width and 2.2 mm depth was made on the surface of workpieces and then filled by powders before FSP. The FSP tool was made of H13 alloy and was exposed to the heat treatment to achieve a hardness of 54 HRC. The tool's pin had a triangular shape by 5.4 mm length and 5 mm diameter, and the flat shoulder diameter was 20 mm. The traveling and the rotational speed of FSP were chosen 25 mm/min and 800 rpm, respectively. The tilt angle during FSP was 3° and was applied in the same positions in all deformation passes. An argon atmosphere was used as the shielding gas under a polycarbonate box around the rotating tool and the workpiece to minimize the surface oxidation during the process. The process was carried out in one and three FSP passes to achieve a uniform distribution of reinforcing particles in the processed zone. Optical microscopy (OM) and electron backscatter diffraction (EBSD) were used to study obtained microstructures, and before OM observations, samples were etched through a solution consists of 4.2 g picric acid, 10 ml distilled water, 70 ml ethanol and 10 ml acetic acid. The samples for EBSD characterization after mechanically grinding polished electrochemically by AC_2 solution. The EBSD measurements were done using a ZEISS

AURIGA© Compact microscope equipped with field emission gun (FEG) and EDAX-EBSD detectors along with the mapping step size of 100 nm. The average grain size and grain distributions are measured by TSL OIM EBSD software.

The fractured surfaces of tensile specimens were observed by scanning electron microscopy (SEM) model Philips XL30. Vickers microhardness of composite specimens was measured using HV-1000A microhardness tester, under loading of 200 g, and a dwell time of 15 s; hardness tests were performed 5 times on various parts of samples' surfaces and then obtained values were averaged. Tensile tests were carried out by using a Santam-20KN universal tester machine by a strain rate of 0.001 s^{-1} at the room temperature.

3. Results and discussions

3.1. Microstructural evolution

Fig. 3 illustrates IPF maps of stir zone microstructures related to AZ31/Gr and AZ31/GNPs composites after one FSP pass. After the first FSP pass, an equiaxed microstructure (Fig. 3a) with the average size (Fig. 3c) of 12.23 µm is obtained for AZ31/Gr composite. In the case of AZ31/GNP composite (Fig. 2d), a microstructure consists of grains with an average size of 10.13 µm (Fig. 3f) is achieved. As can be seen in Fig. 3b and Fig. 3e, both Gr and graphene particles have agglomerated in the stir zone and continuous clusters of particles are created. Indeed, because of the weak wetting of carbonaceous materials on the metal substrate, as well as insufficient plastic material flow due to the low heat input in single FSP pass, it is impossible to achieve uniform distribution of particles and clustering/agglomeration of particles is unavoidable. To precisely investigate the distribution of particles, SEM images and also atomic distribution element maps are taken from samples and also point energy-dispersive spectroscopy (EDS) was done to calculate the amount of carbon in certain points. Fig. 4 shows the SEM micrographs and carbon atomic distribution element map for both composites after the first FSP pass. As can be seen, powders did not distribute well in the matrix and clusters of graphite (Fig. 4a, b) and graphene (Fig. 4c, d) are present in the microstructure. The point EDS analysis for both composites also substantiates the high percentage of carbon in points A (AZ31/Gr) and B (AZ31/GNP), which are the clusters. The little difference between the percentage of carbon for AZ31/Gr and AZ31/GNP at clusters indicates that clustering occurred to higher extents in AZ31/Gr composite, compared to AZ31/GNP. By continuing the deformation up to three FSP passes, a different trend is seen. Microstructural evolution after the third FSP pass for both composites is described in Fig. 5. As shown in Fig. 5a and Fig. 5d, a fine uniform microstructure is attained for AZ31/Gr and AZ31/GNP composites, with the average grain sizes of 5.63 and 2.29 µm, respectively. As a matter of fact, the direction of the tool rotation was reversed during the second and third FSP passes and thereby the distribution of particles became more uniform (Fig. 5b, e). The better distribution of particles after the third deformation pass can be observed in Fig. 6. It can be inferred from SEM images (Fig. 6a, c) that the clustering noticeably has decreased for both composites. The EDS analysis also shows that because of the well-distributed particles after the third deformation pass, the percentage (Wt.%) of carbon in clusters (points A and B) has decreased. Again, the distribution of particles is better in the case of AZ31/GNP nanocomposite.

In the first FSP pass for both composites, the grain refinement is mainly due to the FSP processing, not the particles; because agglomerated particles cannot significantly be refined and also cannot restrict the migration of boundaries. Agglomerated graphene nanoplatelets behave approximately as same as graphite micro-size particles. The ultrahigh surface area that can be obtained in nanoplatelets is lost when these sheets become clusters. As can be seen in Fig. 7, clustering of particles (here, clustering of graphite) cannot affect the grain refinement through hindering the grain boundary movement, and this clustering has happened for both composites. Hence, the difference in grain size between AZ31/Gr and AZ31/GNP composites is trivial. In the third FSP pass, particles' distribution and their effect on grain refinement are totally different. In fact, during repeating FSP up to 3-passes, particles' clusters break into smaller pieces as the result of the mechanical breaking due to the applying more strain along with the increase in heat input which thereby facilitates the material and particles flow around the pin. On the other hand, when the FSP tool penetrates into the plate during next passes, the tool would not involve new parts of the material (regions below the stir zone) into the processing zone and all the deformation energy is limited to this processing zone (stir zone). This allows for producing a uniform distribution of reinforcing particles [27]. Consequently, a better distribution of particles is realized after applying 3 FSP passes, as also shown in Fig. 6.

On the other hand, in FSP processing, due to the possibility of imposing large strains, the attainment of very small grains is possible, which occurs through the dynamic recrystallization

(DRX) phenomenon. As a matter of fact, during severe plastic deformation, the grains are broken and a large number of low angle grain boundaries are created. Therefore, suitable places for nucleating DRX grains can be generated [28-31]. Then, the fine nuclei of grains start growing and finally, a microstructure containing fine equiaxed grains is achieved (Fig. 3 and Fig. 5). The existence of more micro and nanoparticles, after the third FSP pass due to the breaking, increases the preferential sites for nucleating DRX grains. So, the average grain size of both composites significantly decreased after 3 FSP passes compared to the pure AZ31 and even the first pass. However, a finer microstructure is achieved for AZ31/GNP composite compared to that of AZ31/Gr. It is believed that in the same volume fraction of reinforcements (micro and nanoparticles), nanosized particles increase the number of particles that provide more nucleation sites [32]; so, the average grain size of AZ31/GNP is finer than that of graphite particles. According to the Zener limiting grain size, finely dispersed particles pin the movement of grain boundaries that are migrating during DRX; therefore, they restrict the grain growth. Zener-Holloman parameter- d_z - [33] ($d_z = \frac{4r}{3v_f}$, where r and v_f are the radii and volume fraction of GNPs particles, respectively) indicates that when the size of particles (r) is reduced or the volume fraction (v_f) increases, the grain size of the substrate becomes finer. As a result, in AZ31/GNPs composite, compared to AZ31/Gr, a finer mean grain size (2.29 μm) can be obtained after 3 FSP passes, due to the finer particles. Accordingly, at 3 FSP passes, due to the absence of clusters and thereby the presence of well-distributed micro and nanoparticles (which is not observed for the 1 FSP pass), grain refinement also occurs as the result of particles by providing preferential sites for nucleating DRX grains (in addition to grain refinement due to FSP); consequently, finer microstructures are achieved compared with 1 FSP pass, particularly for AZ31/GNP composite (Fig. 8).

3.2. Mechanical properties

3.2.1. Hardness measurements

The Vickers microhardness measurements for stir zones of FSP composites reinforced by Gr, and GNPs particles in one and three FSP passes and also the pure AZ31 are shown in Fig. 9. The microhardness profile of FSPed samples at 1 and 3 FSP passes is shown in Fig. 9a. It can be inferred that by going from the center/stir zone toward the base metal, the microhardness variations are more pronounced, especially for AZ31/GNP-3P (after 3 FSP passes). In the stir zone, the variations are negligible and microhardness is higher for all samples, compared to the base metal. As can be seen in Fig. 9b, after imposing one FSP pass, the microhardness increases for both composites (from 54 HV for the pure AZ31 to 58 and 59 HV for AZ31/Gr and AZ31/GNPs, respectively); however, the amount of microhardness increment is insignificant. The difference between the minimum and maximum hardness values implies the inhomogeneous microstructure after one FSP pass due to the formation of agglomerated clusters. For a better demonstration of the inhomogeneity, an inhomogeneity factor (IF) was introduced which is the hardness standard deviation of each sample divided by the average amount of the hardness, and low values of IF means more homogenous microstructure. Fig. 9c shows the IF values for both composites processed by 1 and 3 FSP passes. For AZ31/Gr composite, the microhardness did not increase noticeably even after applying 3 FSP passes (the microhardness increases from 58 HV for 1 FSP pass to 63 HV for the third pass), although a fine microstructure was obtained. However, the IF (Fig. 9c) for AZ31/Gr-3P shows that the microhardness distribution is almost homogenous due to the fact that after applying 3 FSP passes, microparticles are well distributed in the matrix. In fact, graphite particles by weak van der walls forces between their layers are a member of the soft materials group which means that the slip of graphite layers during microhardness measurements prevents from the attainment of remarkable microhardness values [34,35]. Conversely, higher microhardness values of three FSP passes relative to one-pass are because of the broken of graphite layers and their entanglement during the post FSP processing which gave rise to the reduction of the space between layers or the segregation of these layers around the magnesium grains. Nevertheless, the microhardness of the AZ31/GNPs-3P composite (83 HV) remarkably increases compared to both AZ31/GNPs-1P (after 1 pass) and AZ31/Gr-3P, which is also 1.5 times higher than that of pure AZ31 substrate. The notable improvement of AZ31/GNPs composite microhardness at 3 FSP passes can be attributed to the combination of the grain refinement and strengthening by GNPs. It has been previously shown that after 3-FSP passes, the segregation of GNPs particles, due to the mechanical breaking, can effectively retard the grain growth by pinning the boundaries and thereby leads to more grain refinement. Moreover, by the improvement of interfaces of GNPs and Mg substrate, and the creation of a strong interface, the load is effectively transferred to the GNPs particles, thereby, the microhardness increases. It is worthwhile mentioning that the significant grain refinement at 3

FSP passes of AZ31/GNPs composite and the good distribution of GNPs are the major reasons in obtaining a homogenous microstructure, which is also confirmed by the IF value at this deformation pass, which is the lowest among all deformed samples (Fig. 9c).

3.2.2. Tensile properties and fractography

Engineering stress-strain flow curves of AZ31/Gr and AZ31/GNPs composites are depicted in Fig. 10a. As can be observed, after applying one deformation pass, the strength of both composites increased, while the elongation experienced a notable decrease. However, straining up to 3 FSP passes not only increases the strength of both AZ31/Gr and AZ31/GNPs composites but also enhances the elongation, compared to the 1 FSP pass. In both deformations passes, the strength and the elongation of AZ31/GNPs composite are larger than that of graphite. According to Fig. 10b, after one FSP pass, yield strength (YS) of AZ31/Gr and AZ31/GNPs changed from 92 MPa (for pure AZ31) to 110 and 118 MPa, respectively and ultimate tensile strength (UTS) changed from 114 MPa to 120 and 132 MPa for Gr, and GNPs reinforced composites, respectively. Actually, the variation of tensile properties after the first FSP pass is not remarkable in comparison with pure AZ31 due to the agglomeration of both particles which thereby mitigates their strengthening effect. For both reinforcing particles after applying 3 FSP passes, a noticeable improvement in either strength or elongation was realized. YS and UTS increased 48 and 44.73 % in Gr, and also 63 and 68.4 % in GNPs, compared to pure AZ31. This considerable improvement after 3 FSP passes originates from the strengthening mechanisms and the better distribution of particles owing to the mechanical breaking during the process. Generally, the size of reinforcements influences the mechanical properties such as strength, ductility, and fracture of self-lubricant MMCs [36]. Since in microparticles the formation of defects such as cracks is likely during the tensile test and fractured particles cannot bear any tensile load, higher YS and UTS values were obtained for GNPs than Gr. The strengthening mechanisms involved in enhancing the mechanical properties of nanoparticle reinforced metal matrix composites have been completely discussed elsewhere [34]. These mechanisms include the Orowan strengthening, grain and substructure strengthening (Hall–Petch relationship), quench hardening resulting from the dislocations which are generated to accommodate the differential thermal contraction between the reinforcing particles and the matrix, and also the work hardening due to the strain misfit between the elastic reinforcing particles and the plastic matrix [37-41]. In metal matrix nanocomposites (MMNCs) via FSP, the Orowan strengthening mechanism and Hall-Petch relation have the most contribution in strengthening [28], but in MMCs by micro size particles (greater than 1μm), Hall-Petch relation strengthening is dominant, so strengthening through nanoparticles is significantly higher than micro size particles.

Graphite micro-size particles are known as crack initiation sources in composites due to the micro size of particles along with weak van der walls forces between graphite layers, and also weak interface bonding between Gr, and Mg substrate [34,35]. By agglomeration of these particles after one FSP pass, crack initiation sources in the composite during tensile test increase; thus, a reduction in elongation of one FSP pass specimens can be realized, compared with three FSP passes. Fig. 11 indicates the fracture surfaces of pure AZ31 and AZ31/Gr composite processed by one and three FSP passes. AZ31 surface fractography reveals several shallow and wide dimples which are indicative of the cleavage-brittle fracture (Fig. 11a). In Fig. 11b, c, the crack initiation between graphite particles and the laminar fracture on the stir zone are visible after one FSP pass (shown by red arrows), and the material in this region (region A) experiences a brittle fracture due to the crack initiation along agglomerated graphite particles (shown by red arrows in Fig. 11c). After applying 3 FSP passes, due to the better distribution of Gr particles and the relative combination of particles and magnesium substrate, several dimples (red arrows in Fig. 11d) are observable on the fracture surface which illustrate the increscent in elongation of three FSP passes specimens. The EDS analysis for region A (Fig. 11b) and B (Fig. 11d) proves the fact that the crack initiated near the Gr clusters since the percentage of carbon is high (region A); nonetheless, after the third FSP passes, the percentage of carbon decreased in region B showing the dimples, which again implies the better fracture properties of samples processed by 3 FSP passes. Fig. 12 shows fracture surfaces of AZ31/GNPs composite after FSP processing. As can be seen, 1-FSP pass AZ31/GNPs composite (Fig. 12a, b) experienced a brittle and laminar fracture which changed to a fracture surface containing dimples, after the deformation up to 3 passes (Fig. 12c, d). The EDS results also show the high percentage of carbon content for region A (Fig. 12a), where the fracture is because of graphene clusters, while this content dramatically decreased in the region B (Fig. 12c) after three FSP passes, where dimples are the dominant features. The comparison between Fig 11d and Fig 12c demonstrates the increase in the number of dimples all over the fracture surface of AZ31/GNPs composite or in other words, the improved fracture behavior of this composite compared to AZ31/Gr. Because of the improvement in the distribution of GNPs and the increase in the number of grain boundaries (finer grain size) in AZ31/GNPs composite, the brittle characteristic of grain boundaries decreased and an enhancement in the fracture behavior of AZ31/GNPs composite was realized.

4. Conclusion

In the current study, the effect of Gr, and GNPs reinforcement particles on the microstructure and subsequent mechanical properties of AZ31 magnesium alloy were investigated by applying multi-pass FSP. Besides, it is worthwhile mentioning that FSP can be a better candidate to produce magnesium MMCs with successfully improved properties, compared to other surface treatment methods, as shown in this work. Main points resulted from this work can be summarized as follows:

1. The mean grain size of Mg decreased from 40.65 at initial state to 5.63 and 2.29 μm for AZ31/Gr and AZ31/GNPs composites, respectively, after applying three-FSP passes. A finer microstructure was obtained for AZ31/GNP composite due to the Zener limiting grain size, as well as the pinning effect of nanoparticles on grain boundaries.
2. Homogenous microstructures with well-distributed particles were realized after three FSP passes, where the percentage of clusters drastically decreased, especially for graphene nanocomposites.
3. Mechanical properties including Vickers microhardness and UTS of AZ31 magnesium alloy were remarkably improved for both composites after the third FSP pass. A high hardness of 83 HV and UTS of 192 MPa were attained for AZ31/GNP composite.
4. Investigated fracture surfaces implied better fracture properties after imposing 3 FSP passes for both composites, where the brittle fracture of the first pass changed to a combined fracture of brittle-ductile for the Gr, and roughly ductile for the graphene composite.

References

[1] S.C. Tjong, K.C. Lau, Tribological behaviour of SiC particle-reinforced copper matrix composites, Mater. Lett. 43 (2000) 274–280.

[2] Y.W. Wu, K. Wu, K.K. Deng, K.B. Nie, X.J. Wang, X.S. Hu, M.Y. Zheng, Damping capacities and tensile properties of magnesium matrix composites reinforced by graphite particles, Mater. Sci. Eng. A. 527 (2010) 6816–6821.

[3] I.A. Ovid'ko, Metal-graphene nanocomposites with enhanced mechanical properties: a review., Rev. Adv. Mater. Sci. 38 (2014).

[4] W. Ames, A.T. Alpas, Wear mechanisms in hybrid composites of graphite-20 Pct SiC in A356 aluminum alloy (Al-7 Pct Si-0.3 Pct Mg), Metall. Mater. Trans. A. 26 (1995) 85–98.

[5] J.B. Yang, C.B. Lin, T.C. Wang, H.Y. Chu, The tribological characteristics of A356. 2Al alloy/Gr (p) composites, Wear. 257 (2004) 941–952.

[6] H. Sarmadi, A.H. Kokabi, S.M.S. Reihani, Friction and wear performance of copper–graphite surface composites fabricated by friction stir processing (FSP), Wear. 304 (2013) 1–12.

[7] K. Landry, S. Kalogeropoulou, N. Eustathopoulos, Wettability of carbon by aluminum and aluminum alloys, Mater. Sci. Eng. A. 254 (1998) 99–111.

[8] L.-Y. Chen, H. Konishi, A. Fehrenbacher, C. Ma, J.-Q. Xu, H. Choi, H.-F. Xu, F.E. Pfefferkorn, X.-C. Li, Novel nanoprocessing route for bulk graphene nanoplatelets reinforced metal matrix nanocomposites, Scr. Mater. 67 (2012) 29–32.

[9] M.A. Rafiee, J. Rafiee, Z. Wang, H. Song, Z.-Z. Yu, N. Koratkar, Enhanced mechanical properties of nanocomposites at low graphene content, ACS Nano. 3 (2009) 3884–3890.

[10] R. Sengupta, M. Bhattacharya, S. Bandyopadhyay, A.K. Bhowmick, A review on the mechanical and electrical properties of graphite and modified graphite reinforced polymer composites, Prog. Polym. Sci. 36 (2011) 638–670.

[11] P. Song, Z. Cao, Y. Cai, L. Zhao, Z. Fang, S. Fu, Fabrication of exfoliated graphene-based polypropylene nanocomposites with enhanced mechanical and thermal properties, Polymer (Guildf). 52 (2011) 4001–4010.

[12] S.C. Tjong, Recent progress in the development and properties of novel metal matrix nanocomposites reinforced with carbon nanotubes and graphene nanosheets, Mater. Sci. Eng. R Reports. 74 (2013) 281–350.

[13] J.D. Majumdar, B.R. Chandra, R. Galun, B.L. Mordike, I. Manna, Laser composite surfacing of a magnesium alloy with silicon carbide, Compos. Sci. Technol. 63 (2003) 771–778.

[14] S.R. Bakshi, A.K. Keshri, A. Agarwal, A comparison of mechanical and wear properties of plasma sprayed carbon nanotube reinforced aluminum composites at nano and macro scale, Mater. Sci. Eng. A. 528 (2011) 3375–3384.

[15] R.S. Mishra, Z.Y. Ma, Friction stir welding and processing, Mater. Sci. Eng. R Reports. 50 (2005) 1–78.

[16] M. Klich, W. Tuta, K. Kyzioł, P. Kuoetrowski, D. Batory, W. Szymañski, M. Stegliñski, D. Kottfer, Influence of the Chemical Composition of Al/AlC/a-C: H Coatings on the Mechanical Properties of Magnesium Alloy AZ31, Met. Sci. Heat Treat. 60 (2018) 443–449.

[17] K. Kyzioł, K. Koper, Ł. Kaczmarek, Z. Grzesik, Plasmochemical modification of aluminum-zinc alloys using NH3-Ar atmosphere with anti-wear coatings deposition, Mater. Chem. Phys. 189 (2017) 198–206.

[18] İ. Çelik, Structure and surface properties of Al2O3–TiO2 ceramic coated AZ31 magnesium alloy, Ceram. Int. 42 (2016) 13659–13663.

[19] R.S. Mishra, M.W. Mahoney, S.X. McFadden, N.A. Mara, A.K. Mukherjee, High strain rate superplasticity in a friction stir processed 7075 Al alloy, Scr. Mater. 42 (1999) 163–168.

[20] R.S. Mishra, M.W. Mahoney, Friction stir processing: a new grain refinement technique to achieve high strain rate superplasticity in commercial alloys, in: Mater. Sci. Forum, Trans Tech Publ, 2001: pp. 507–514.

[21] R.S. Mishra, Z.Y. Ma, I. Charit, Friction stir processing: a novel technique for fabrication of surface composite, Mater. Sci. Eng. A. 341 (2003) 307–310.

[22] Y. Morisada, H. Fujii, T. Nagaoka, M. Fukusumi, MWCNTs/AZ31 surface composites fabricated by friction stir processing, Mater. Sci. Eng. A. 419 (2006) 344–348.

[23] Y. Morisada, H. Fujii, T. Nagaoka, M. Fukusumi, Effect of friction stir processing with SiC particles on microstructure and hardness of AZ31, Mater. Sci. Eng. A. 433 (2006) 50–54.

[24] C.J. Lee, J.C. Huang, P.J. Hsieh, Mg based nano-composites fabricated by friction stir processing, Scr. Mater. 54 (2006) 1415–1420.

[25] A. Shafiei-Zarghani, S.F. Kashani-Bozorg, A. Zarei-Hanzaki, Microstructures and mechanical properties of Al/Al 2 O 3 surface nano-composite layer produced by friction stir processing, Mater. Sci. Eng. A. 500 (2009) 84–91.

[26] M. Balakrishnan, I. Dinaharan, R. Palanivel, R. Sivaprakasam, Synthesize of AZ31/TiC magnesium matrix composites using friction stir processing, J. Magnes. Alloy. 3 (2015) 76–78.

[27] S. Sahraeinejad, H. Izadi, M. Haghshenas, A.P. Gerlich, Fabrication of metal matrix composites by friction stir processing with different particles and processing parameters, Mater. Sci. Eng. A. 626 (2015) 505–513.

[28] C. CI, P. HR, H. JC, On the hardening of friction stir processed Mg-AZ31 based composites with 5–20% nano-ZrO2 and nano-SiO2 particles, Mater. Trans. 47 (2006) 2942–2949.

[29] A. Salandari-Rabori, A. Zarei-Hanzaki, S.M. Fatemi, M. Ghambari, M. Moghaddam, Microstructure and superior mechanical properties of a multi-axially forged WE magnesium alloy, J. Alloys Compd. 693 (2017) 406–413.

[30] A. Salandari-Rabori, A. Zarei-Hanzaki, H.R. Abedi, J.S. Lecomte, H. Khatami-Hamedani, Micro and macro texture evolution during multiaxial forging of a WE43 magnesium alloy, J. Alloys Compd. 739 (2018) 249–259. doi:10.1016/j.jallcom.2017.12.181.

[31] M. Azimi, S.S. Mirjavadi, A. Salandari-Rabori, Effect of temperature on microstructural evolution and subsequent enhancement of mechanical properties in a backward extruded magnesium alloy, Int. J. Adv. Manuf. Technol. 95 (2018) 3155–3166.

doi:10.1007/s00170-017-1343-5.

[32] G. Faraji, O. Dastani, S.A.A.A. Mousavi, Effect of process parameters on microstructure and micro-hardness of AZ91/Al2O3 surface composite produced by FSP, J. Mater. Eng. Perform. 20 (2011) 1583–1590.

[33] P. Asadi, G. Faraji, A. Masoumi, M.K.B. Givi, Experimental investigation of magnesium-base nanocomposite produced by friction stir processing: effects of particle types and number of friction stir processing passes, Metall. Mater. Trans. A. 42 (2011) 2820–2832.

[34] A.M. Asl, S.T. Khandani, Role of hybrid ratio in microstructural, mechanical and sliding wear properties of the Al5083/Graphite p/Al 2 O 3p a surface hybrid nanocomposite fabricated via friction stir processing method, Mater. Sci. Eng. A. 559 (2013) 549–557.

[35] S. Bansal, J.S. Saini, Mechanical and Wear Properties of SiC/Graphite Reinforced Al359 Alloy-based Metal Matrix Composite., Def. Sci. J. 65 (2015).

[36] A.D. Moghadam, E. Omrani, P.L. Menezes, P.K. Rohatgi, Mechanical and tribological properties of self-lubricating metal matrix nanocomposites reinforced by carbon nanotubes (CNTs) and graphene–a review, Compos. Part B Eng. 77 (2015) 402–420.

[37] M. Habibnejad-Korayem, R. Mahmudi, W.J. Poole, Enhanced properties of Mg-based nano-composites reinforced with Al 2 O 3 nano-particles, Mater. Sci. Eng. A. 519 (2009) 198–203.

[38] S.M. Ramezani, A. Zarei-Hanzaki, H.R. Abedi, A. Salandari-Rabori, P. Minarik, Achievement of fine-grained bimodal microstructures and superior mechanical properties in a multi-axially forged GWZ magnesium alloy containing LPSO structures, J. Alloys Compd. 793 (2019) 134–145.

[39] A. M. Jamili, A. Zarei-Hanzaki, H. R. Abedi, P. Minárik, R. Soltani, The microstructure, texture, and room temperature mechanical properties of friction stir processed Mg-Y-Nd alloy, Mater. Sci. Eng. A. 690 (2017) 244-253.

[40] N. Haghdadi, A. Zarei-Hanzaki, H. R. Abedi, D. Abou-Ras, M. Kawasaki, A. P. Zhilyaev, Evolution of microstructure and mechanical properties in a hypoeutectic Al–Si–Mg alloy processed by accumulative back extrusion, Mater. Sci. Eng. A. 651 (2016) 269-279.

[41] H. Khoshzaban Khosroshahi, F. Fereshteh Saniee, H. R. Abedi, Mechanical properties improvement of cast AZ80 Mg alloy/nano-particles composite via thermomechanical processing, Mater. Sci. Eng. A. 595 (2014) 284-290.

Figures' captions

Fig. 1. (a) Inverse pole figure map of pure AZ31, (b) corresponding grain size distribution, and (c) schematic representative of FSP.

Fig. 2. SEM micrographs of particles: (a) Gr microparticles and (b, c) GNPs.

Fig. 3. (a, d) Inverse pole figure maps, (b, e) OM, and (c, f) grain size distribution of AZ31/Gr, and AZ31/GNP after one FSP pass, respectively. Both IPF and OM are from stir zone.

Fig. 4. Stir zone SEM micrographs of AZ31/Gr composite after (a) 1 FSP pass and (b) corresponding carbon atomic distribution element map, and after (c) 3 FSP passes and (d) corresponding carbon element map.

Fig. 5. (a, d) Inverse pole figure maps, (b, e) OM, and (c, f) grain size distribution of AZ31/Gr, and AZ31/GNP after three FSP passes, respectively. Both IPF and OM are from stir zone.

Fig. 6. Stir zone SEM micrographs of AZ31/GNP composite after (a) 1 FSP pass and (b) corresponding carbon atomic distribution element map, and after (c) 3 FSP passes and (d) corresponding carbon element map.

Fig. 7. The graphite cluster after one FSP pass of AZ31/Gr composite.

Fig. 8. The grain size variation for pure AZ31 and AZ31/Gr and AZ31/GNP composites.

Fig. 9. (a) Microhardness profile of undeformed and deformed samples, (b) microhardness variations, and (c) inhomogeneity factor. (b, c) are for stir zone.

Fig. 10. (a) Engineering stress vs. engineering strain flow curves of pure AZ31 and composites materials, and (b) tensile properties of pure and AZ31/Gr and AZ31/GNP composites.

Fig. 11. Fracture surfaces of (a) pure AZ31, and AZ31/Gr composite after (b, c) one FSP pass, (d, e) three FSP passes.

Fig. 12. Fracture surfaces of AZ31/GNP after (a, b) first FSP pass, and (c, d) third FSP pass.

Tables' captions

Table 1. The chemical composition of experimental AZ31 magnesium alloy

Table 1. The chemical composition of experimental AZ31 magnesium alloy

Al (wt. %)	**Zn**	**Mn**	**Ca**	**Cu**	**Ni**	**Fe**	**Mg**
2.98	0.81	0.35	0.02	0.02	0.01	0.01	Bal.

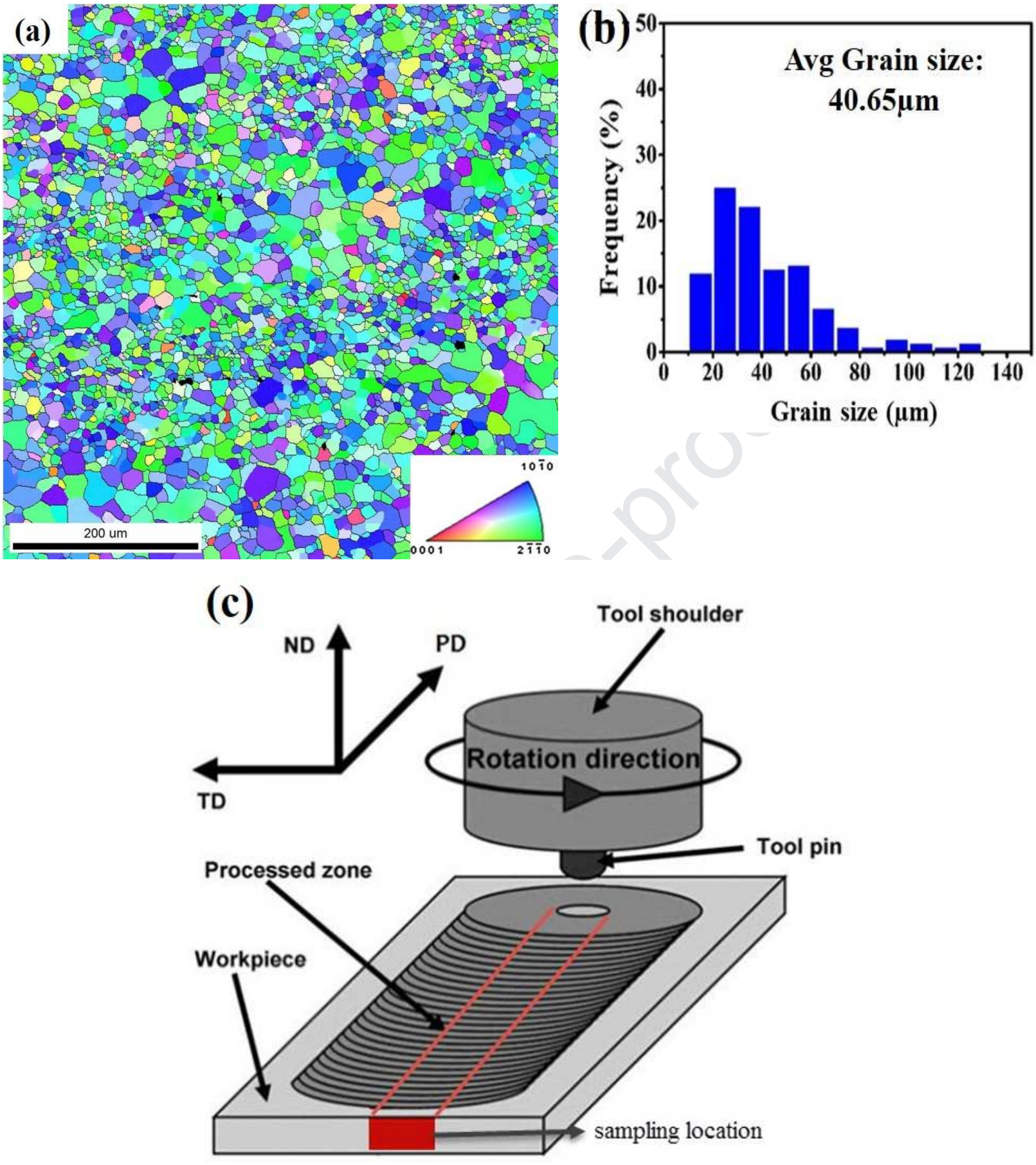

Fig. 1. (a) Inverse pole figure map of pure AZ31, (b) corresponding grain size distribution, and (c) schematic representative of FSP.

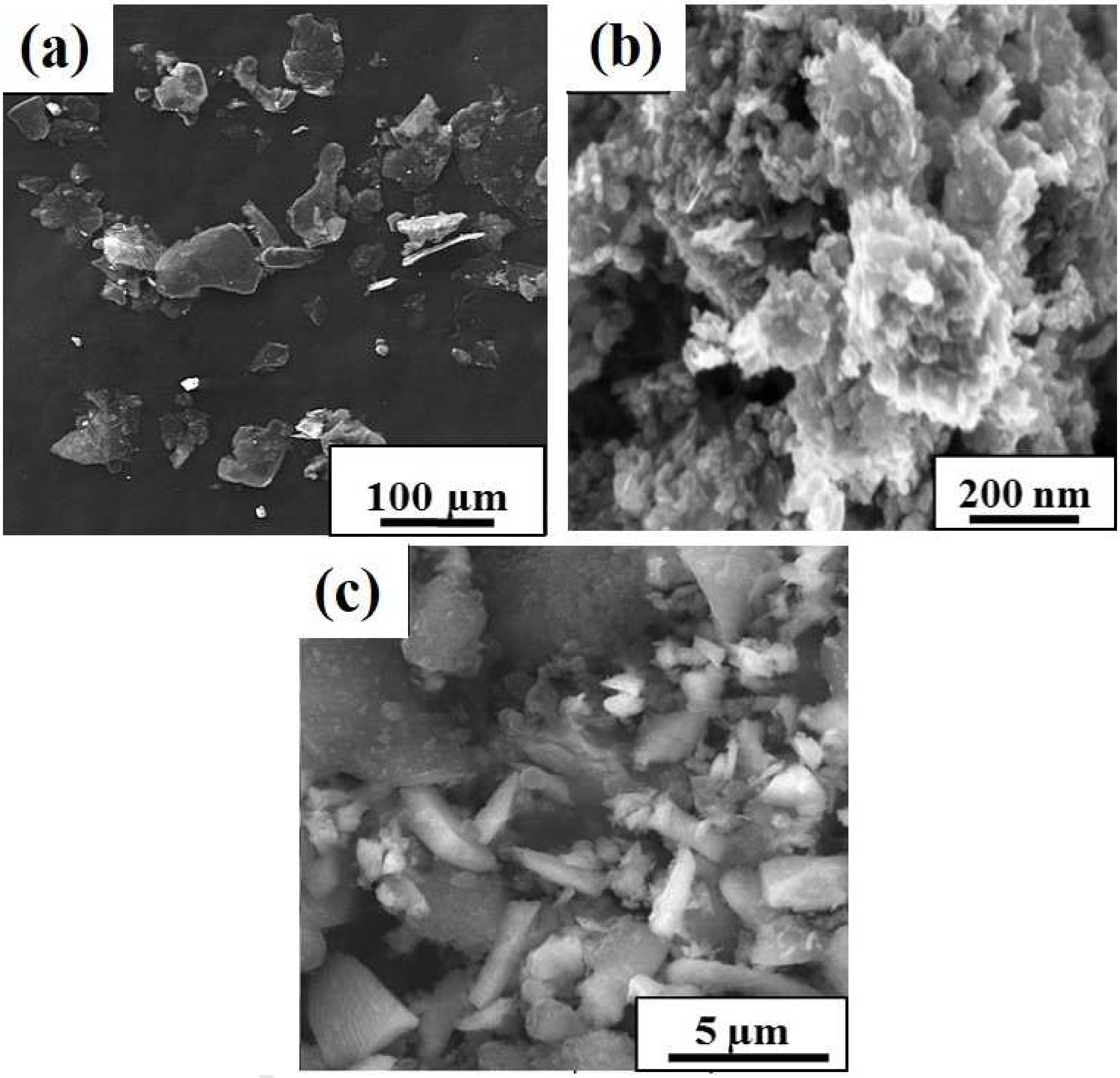

Fig. 2. SEM micrographs of particles: (a) Gr microparticles and (b, c) GNPs.

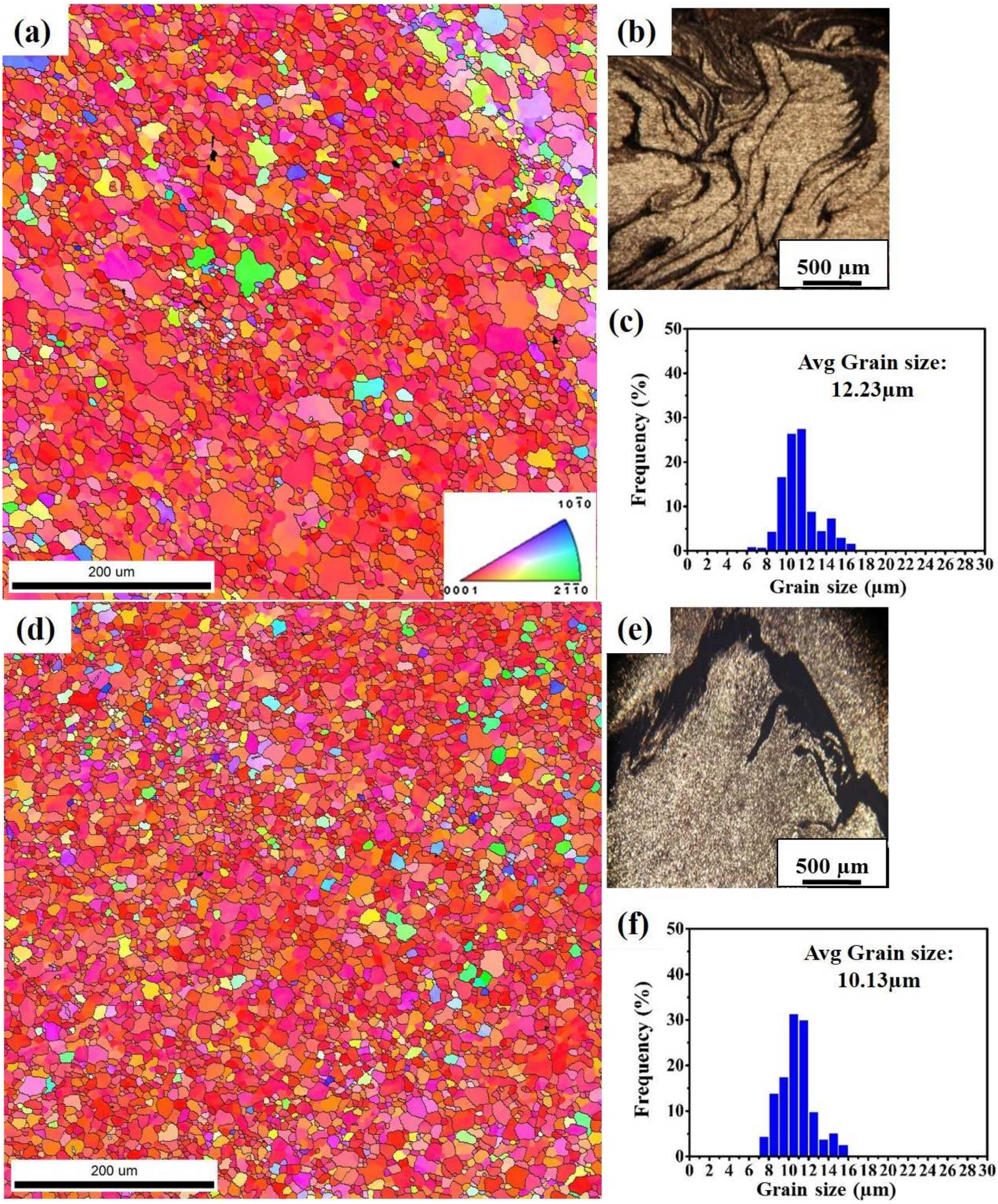

Fig. 3. (a, d) Inverse pole figure maps, (b, e) OM, and (c, f) grain size distribution of AZ31/Gr, and AZ31/GNP after one FSP pass, respectively. Both IPF and OM are from stir zone.

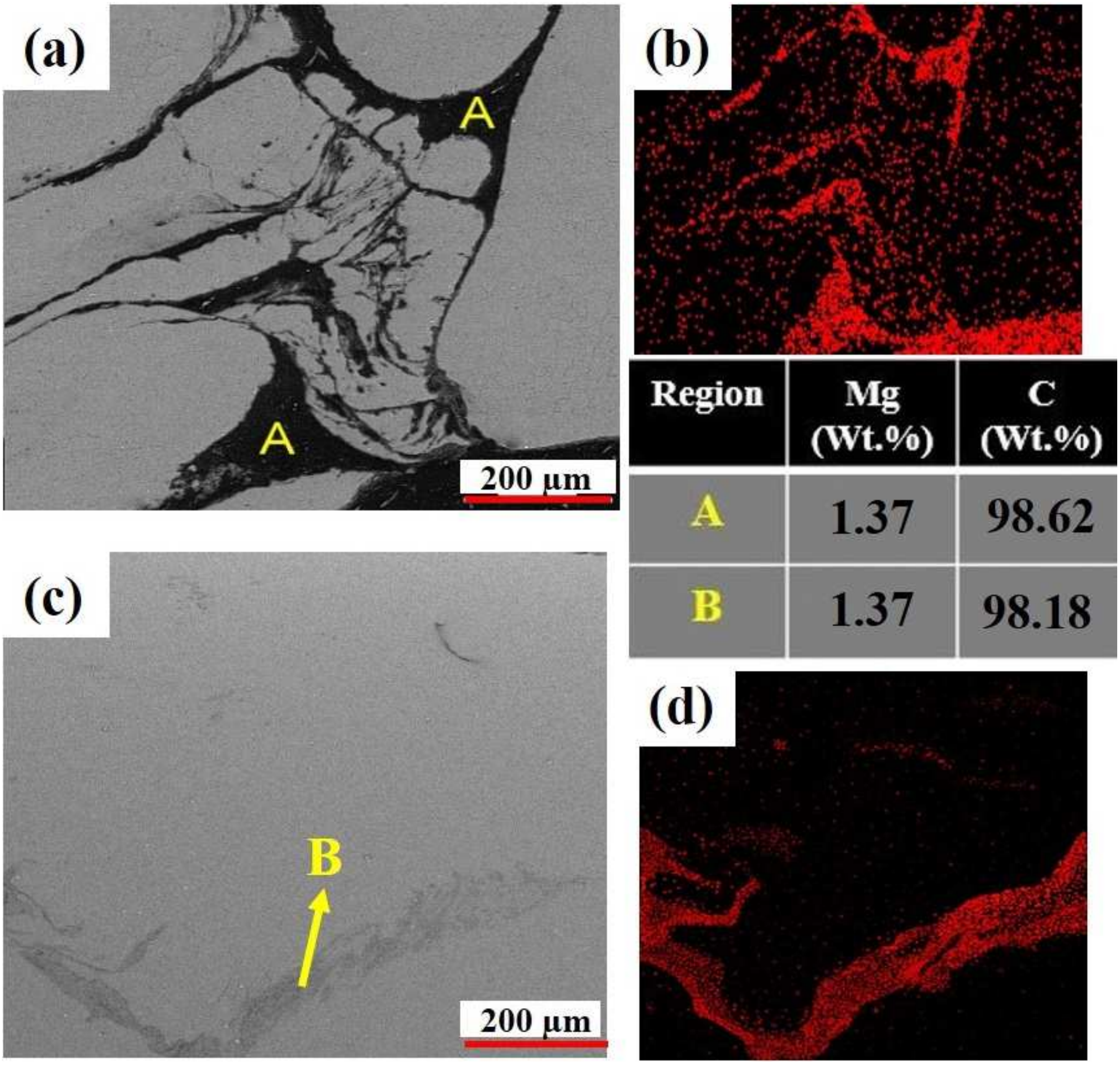

Region	Mg (Wt.%)	C (Wt.%)
A	1.37	98.62
B	1.37	98.18

Fig. 4. Stir zone SEM micrographs of AZ31/Gr composite after (a) 1 FSP pass and (b) corresponding carbon atomic distribution element map, and after (c) 3 FSP passes and (d) corresponding carbon element map.

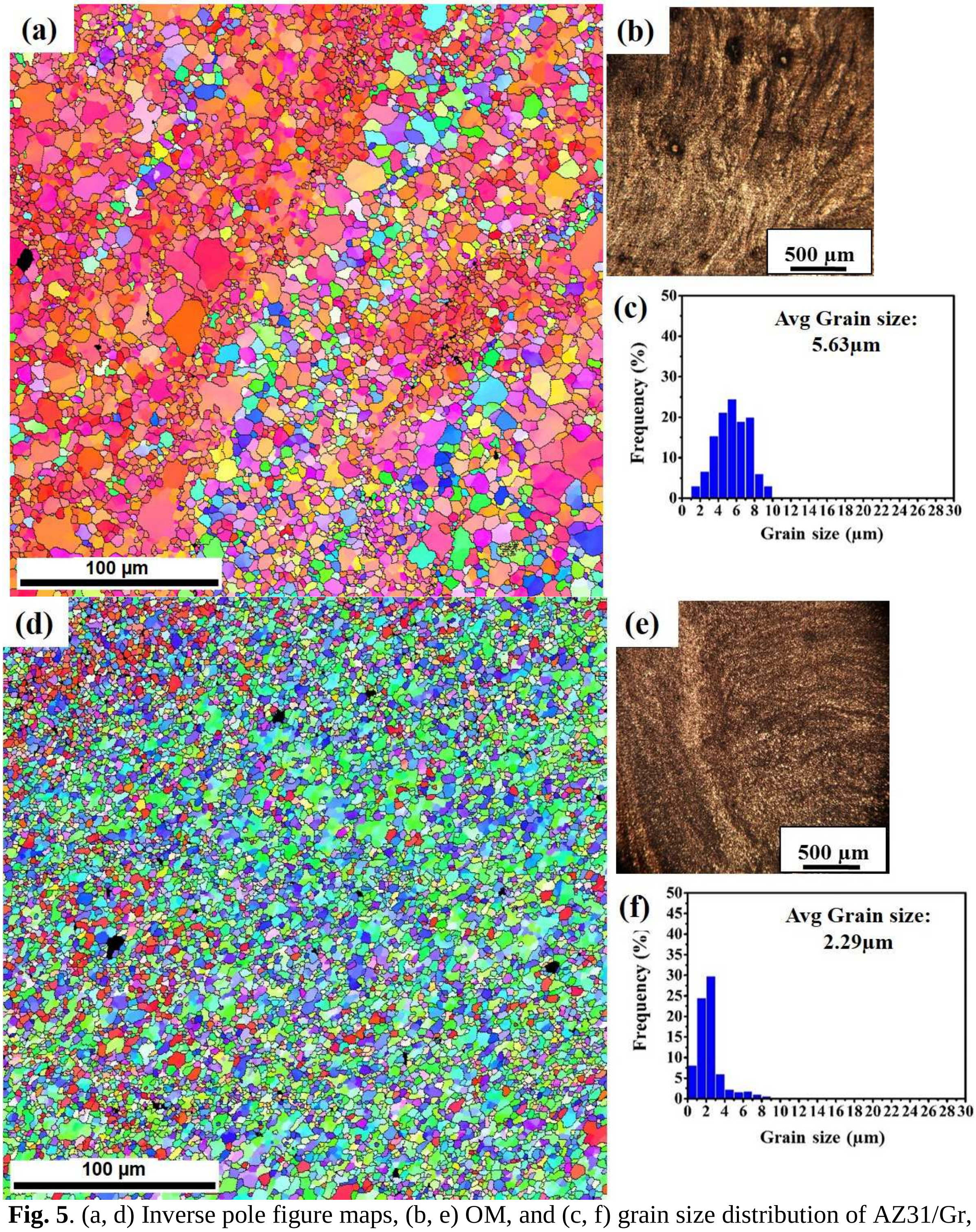

Fig. 5. (a, d) Inverse pole figure maps, (b, e) OM, and (c, f) grain size distribution of AZ31/Gr, and AZ31/GNP after three FSP passes, respectively. Both IPF and OM are from stir zone.

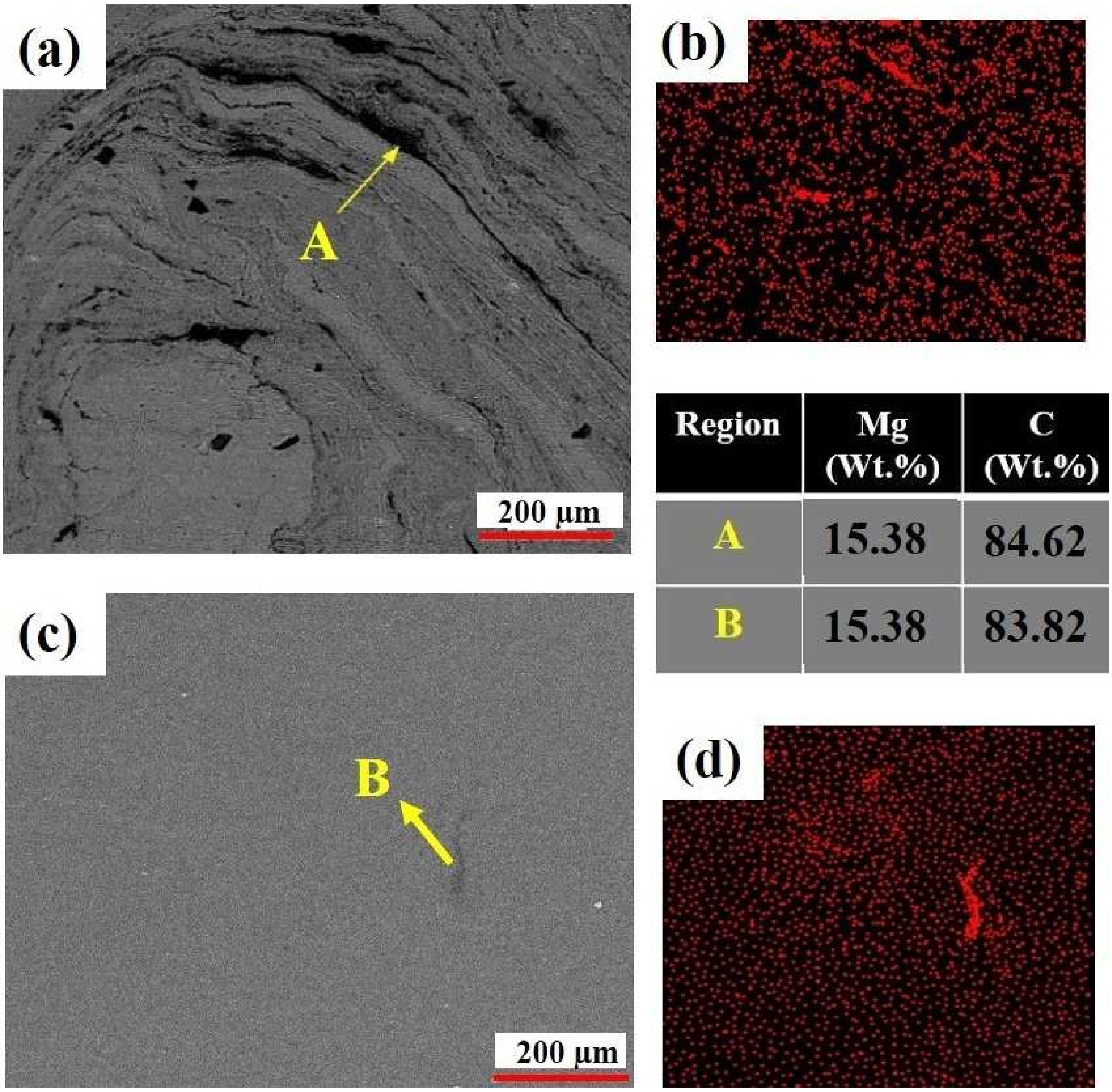

Region	Mg (Wt.%)	C (Wt.%)
A	15.38	84.62
B	15.38	83.82

Fig. 6. Stir zone SEM micrographs of AZ31/GNP composite after (a) 1 FSP pass and (b) corresponding carbon atomic distribution element map, and after (c) 3 FSP passes and (d) corresponding carbon element map.

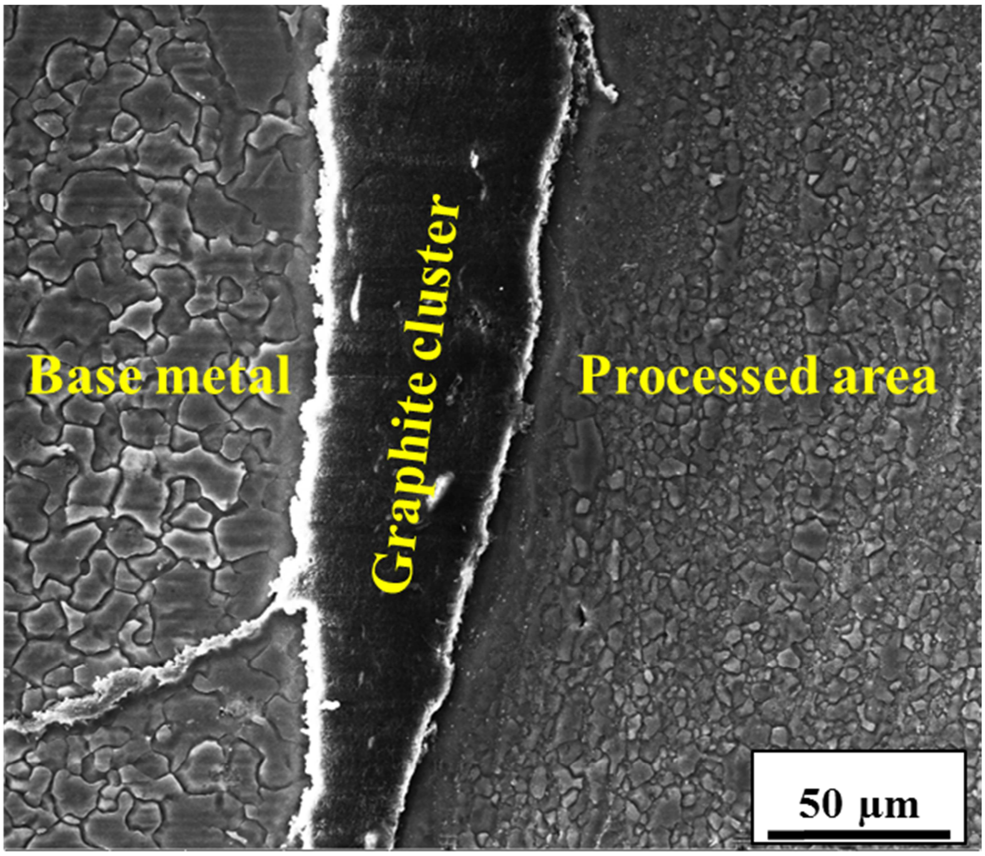

Fig. 7. The graphite cluster after one FSP pass of AZ31/Gr composite.

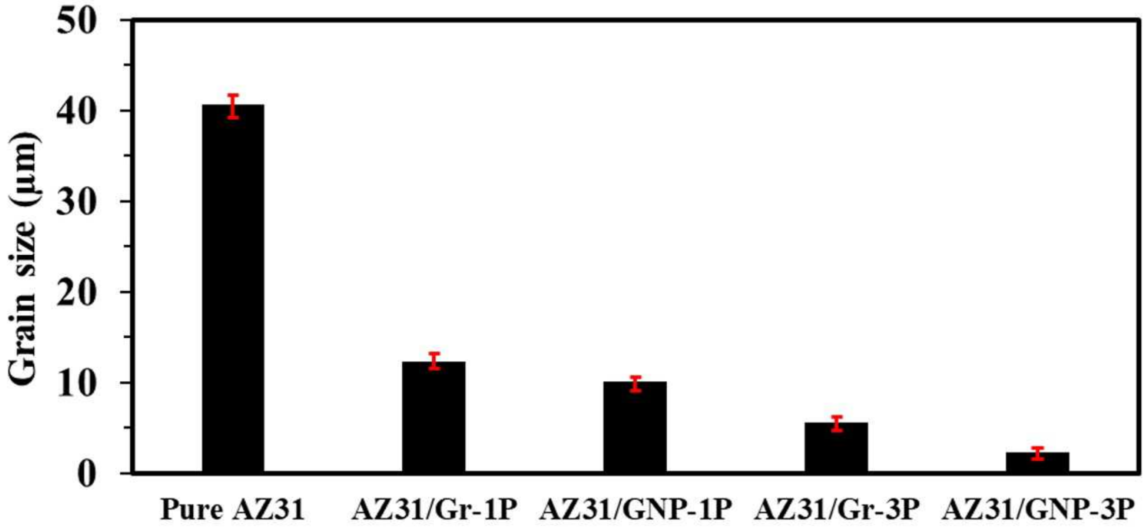

Fig. 8. The grain size variation for pure AZ31 and AZ31/Gr and AZ31/GNP composites.

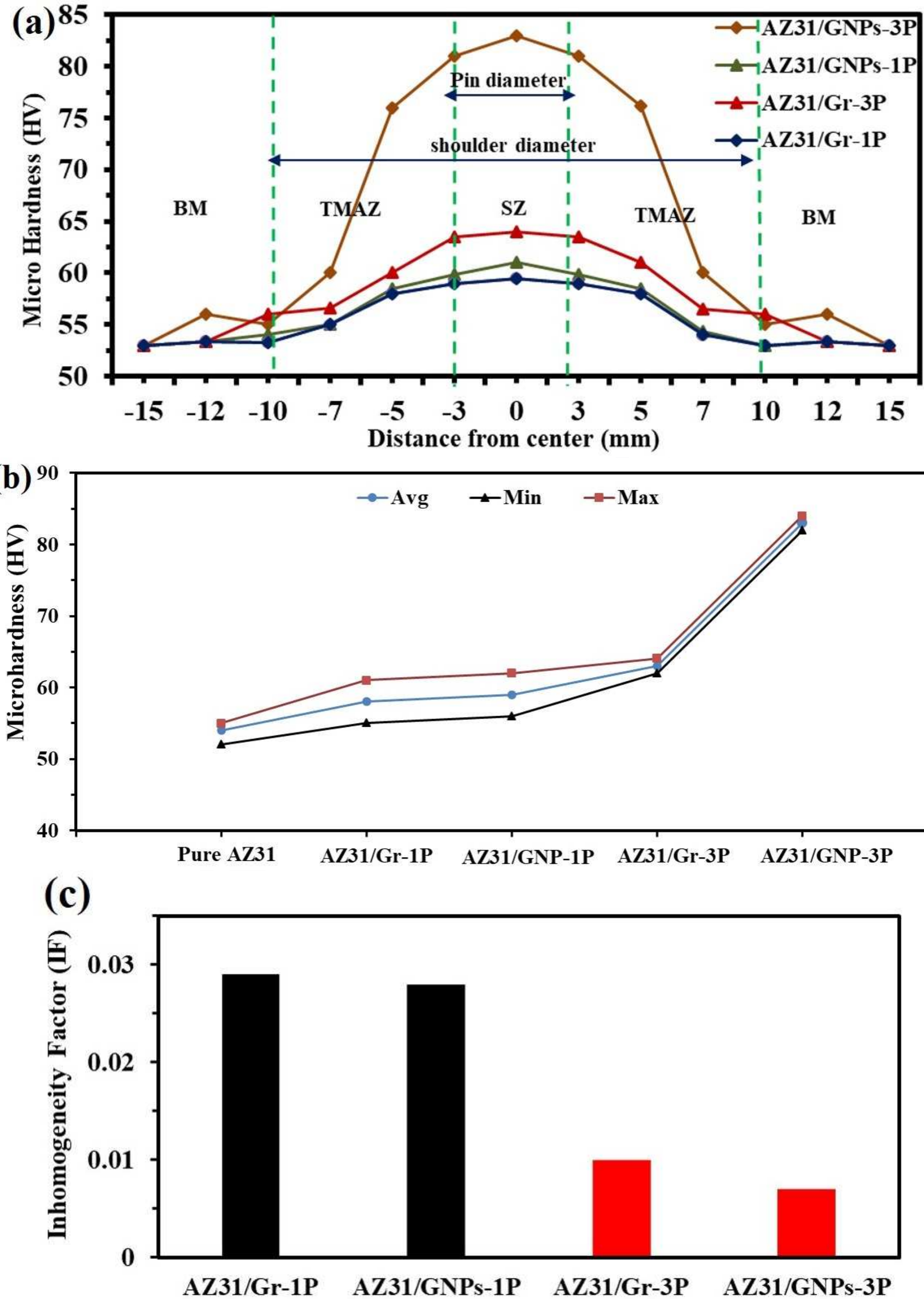

Fig. 9. (a) Microhardness profile of undeformed and deformed samples, (b) microhardness variations, and (c) inhomogeneity factor. (b, c) are for stir zone.

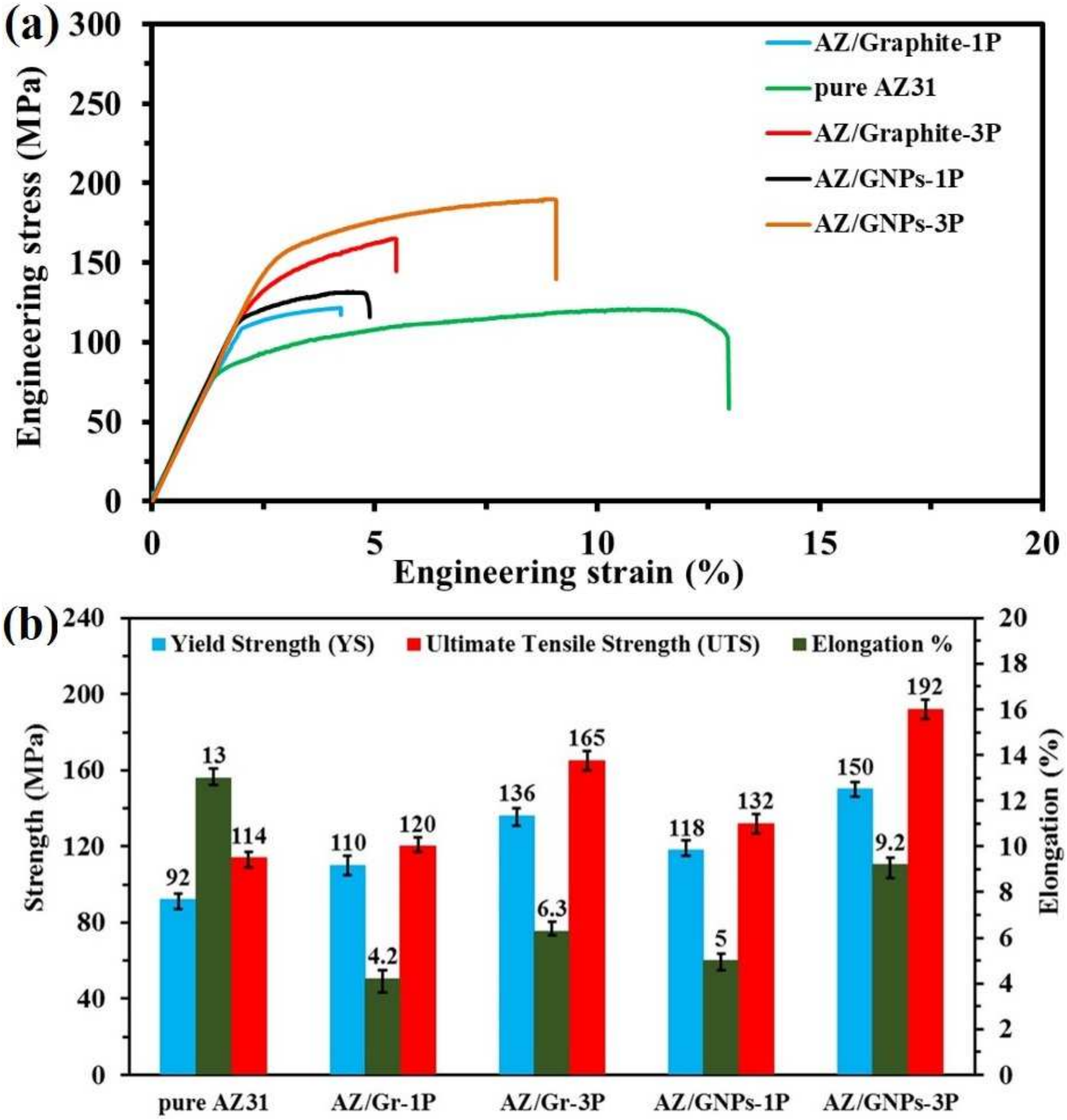

Fig. 10. (a) Engineering stress vs. engineering strain flow curves of pure AZ31 and composites materials, and (b) tensile properties of pure and AZ31/Gr and AZ31/GNP composites.

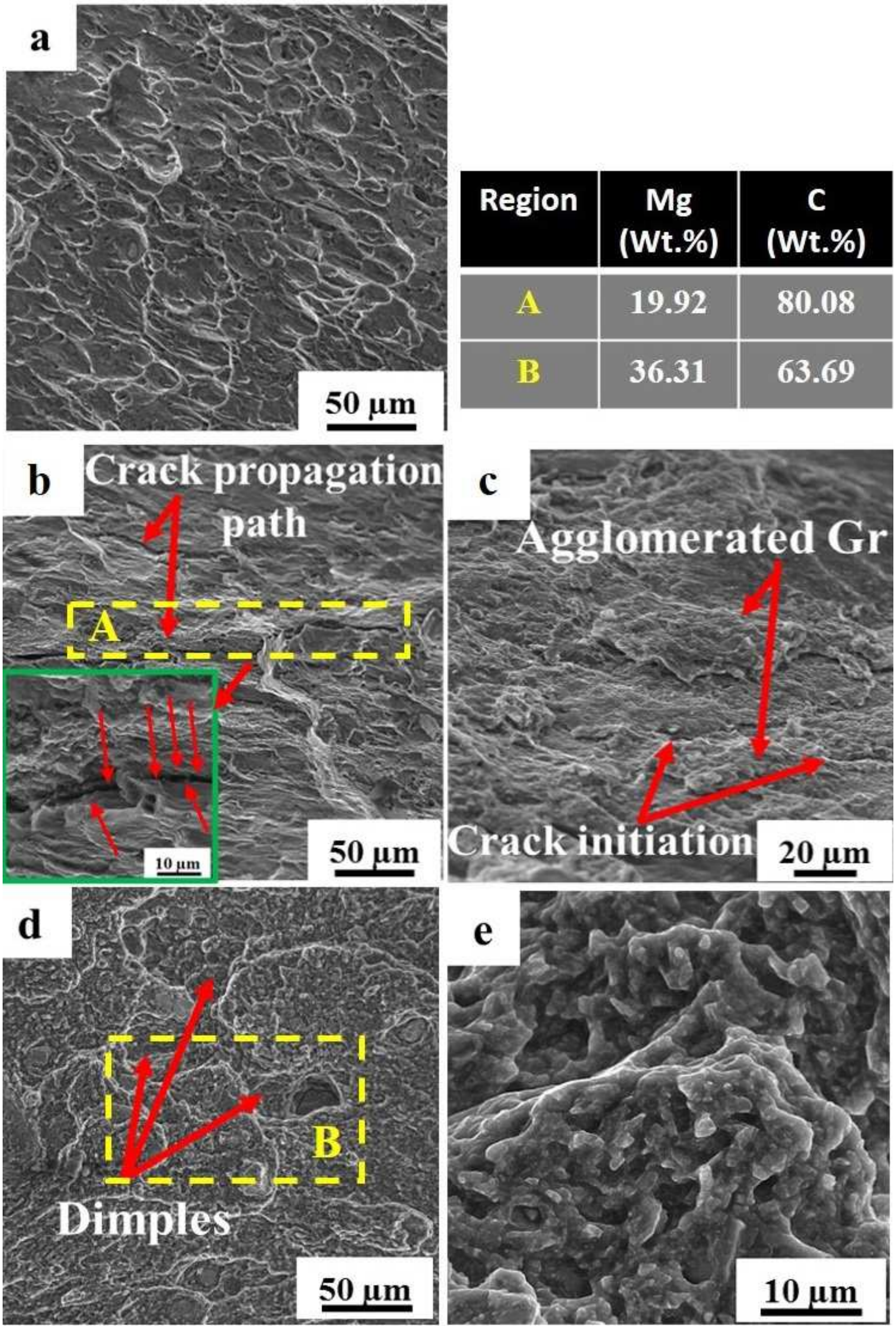

Region	Mg (Wt.%)	C (Wt.%)
A	19.92	80.08
B	36.31	63.69

Fig. 11. Fracture surfaces of (a) pure AZ31, and AZ31/Gr composite after (b, c) one FSP pass, (d, e) three FSP passes.

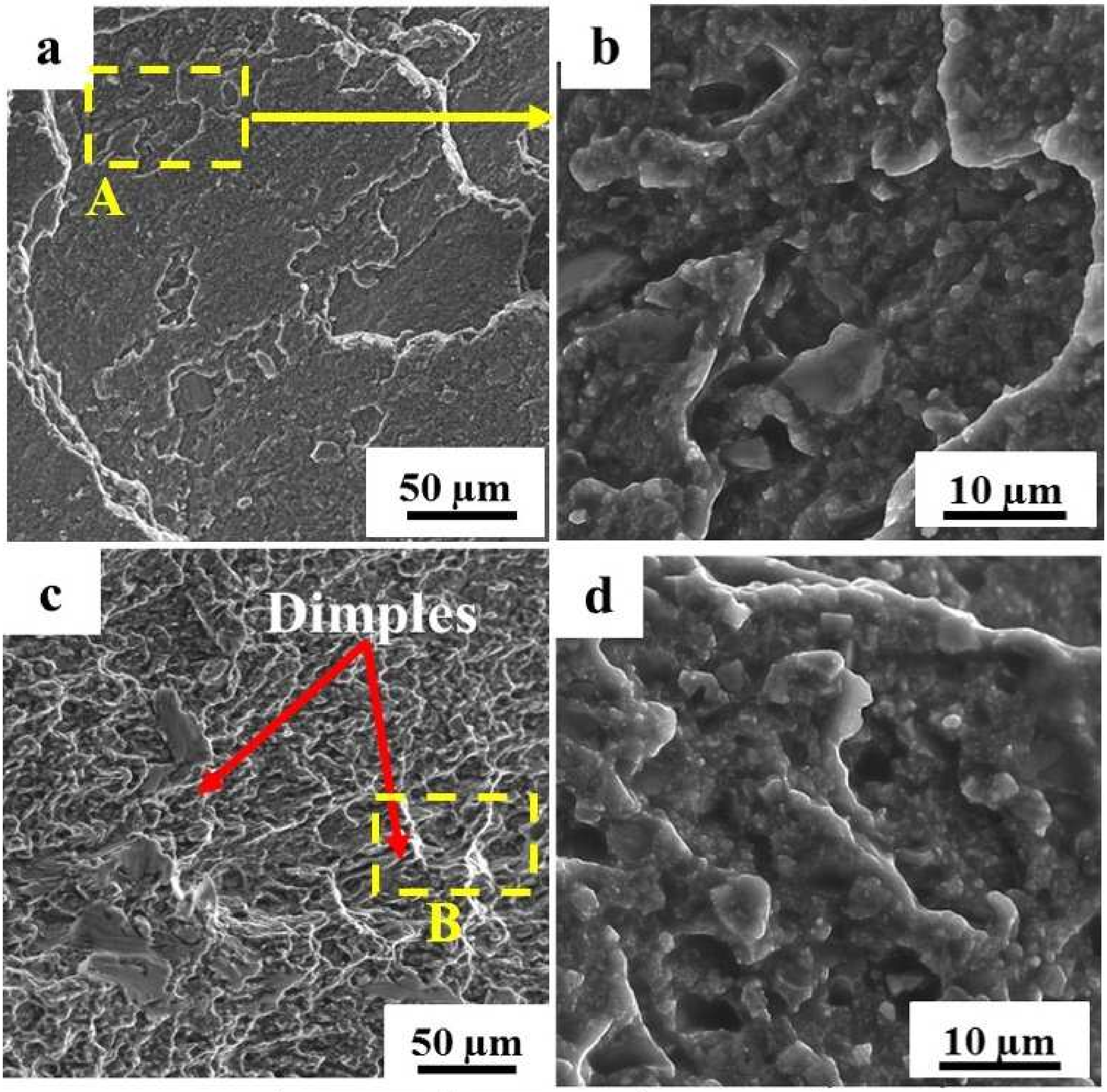

Region	Mg (Wt.%)	C (Wt.%)
A	17.87	82.13
B	43.73	56.27

Fig. 12. Fracture surfaces of AZ31/GNP after (a, b) first FSP pass, and (c, d) third FSP pass.

Highlights

- Fabrication of metal matric composites through friction stir processing
- Homogenous and well-distribution of nano-graphene and micro-graphite particles
- The pinning effect of nano particles and achievement of ultrafine microstructures
- Remarkably improvement of the mechanical properties for both composites
- Brittle fracture of first pass processed specimen changes to mixed mode at third pass